Available online at www.sciencedirect.com
ScienceDirect
Acta Materialia 56 (2008) 5–15
Acta MATERIALIA
www.elsevier.com/locate/actamat

Non-Schmid behaviour during secondary twinning in a polycrystalline magnesium alloy

M.R. Barnett *, Z. Keshavarz, A.G. Beer, X. Ma

ARC Centre of Excellence for Design in Light Metals, CMFI, Deakin University, Geelong, Australia

Received 4 June 2007; received in revised form 17 August 2007; accepted 19 August 2007
Available online 5 November 2007

Abstract

The present work combines electron backscattering diffraction and Schmid analysis to investigate secondary twinning in the magnesium alloy Mg–3Al–1Zn. Inspection of the misorientations between the parent and $\{10\bar{1}1\}$–$\{10\bar{1}2\}$ doubly twinned volumes reveals that there are four possible variants. One of these variants (the one that forms a misorientation with the matrix characterized by 38° $\langle 1\bar{2}10\rangle$) is favoured much more than the others. This variant involves the activation of secondary twinning systems quite inconsistent with Schmid-type behaviour. For the secondary twin to grow significantly it must take on a shape enforced by the primary twin. This is non-optimal for strain compatibility. It is argued that the 38° $\langle 1\bar{2}10\rangle$ variant occurs most because it provides the closest match between the primary and secondary twinning planes, thus minimizing the compatibility strain.

Keywords: Magnesium; Twinning; Schmid factor; Non-Schmid

1. Introduction

It has long been recognized that the mechanical behaviour of magnesium single crystals is sensitive to the nature of the mechanical twins that form [1–4]. Compression perpendicular to the *hcp c*-axis favours the formation of twins on the $\{10\bar{1}2\}$ plane and while this is occurring the flow stress remains low and displays little work hardening [1]. Compression along the *c*-axis favours other twinning modes due to the polarity of twinning. Although different modes have been observed by a number of authors (e.g. [5,6]), it is quite common for twinning to occur on the $\{10\bar{1}1\}$ plane [2]. In many cases this is followed by "re-twinning" or "secondary" twinning on the $\{10\bar{1}2\}$ plane. Rapid flow localization and failure then shortly ensues [2]. There is increasing evidence [7,8] for the suggestion made by Couling et al. in the 1950s [9] that a similar phenomenon to this determines the ductile failure in polycrystals. The present communication is concerned with secondary twinning inside primary $\{10\bar{1}1\}$ twins in polycrystalline Mg–3Al–1Zn (AZ31), the most common wrought magnesium alloy.

The reason $\{10\bar{1}1\}$–$\{10\bar{1}2\}$ double twinning leads to localization and failure in single crystals is that it rotates the basal plane into a position where it is much more favourably oriented for glide. This reorientation of the basal plane was illustrated elegantly by Hartt and Reed-Hill in 1968 [10] using surface replica analysis and we have reproduced a version of their diagram in Fig. 1. The more favourable alignment of the basal slip plane is shown; so too is the development of secondary $\{10\bar{1}2\}$ twinning in the primary $\{10\bar{1}1\}$ interior. The primary $\{10\bar{1}1\}$ twin reorients the basal plane by ~56° around a $\langle 1\bar{2}10\rangle$ axis; in this case, the secondary $\{10\bar{1}2\}$ twin rotates the basal pole "back" by ~86° around the same axis and the net result is a reorientation of the original *c*-axis by 38° around the $\langle 1\bar{2}10\rangle$ axis [2].

With the advent of electron backscattering diffraction (EBSD) it is, in principle, a fairly straightforward matter to seek for boundaries characterized by this misorientation

* Corresponding author. Tel.: +61 3 5227 2797; fax: +61 3 5227 1103.
E-mail address: barnettm@deakin.edu.au (M.R. Barnett).

1359-6454/$30.00
doi:10.1016/j.actamat.2007.08.034

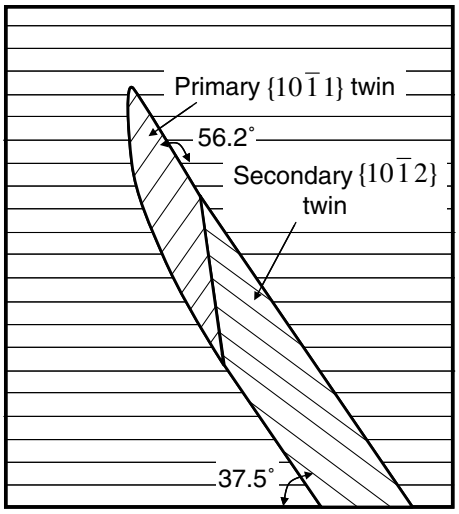

Fig. 1. Schematic of a double $\{10\bar{1}1\}$–$\{10\bar{1}2\}$ twin based on Hartt and Reed-Hill's [10] analysis of a replica taken from a single crystal. The crosshatching lines correspond to basal plane traces and the image zone axis is a $\langle 1\bar{2}10\rangle$ axis.

relationship in polycrystalline material. However, in practice, the interiors of these double twins are not always readily indexed and this hampers their identification. Nevertheless, an increasing number of workers have used EBSD to detect the 38° $\langle 1\bar{2}10\rangle$ double twinning relation in samples of sheet and extruded material [11,12]. Similar findings have been reported by some of the present authors for compression along the predominant basal pole orientation [8] and in the cold rolling of sheet [7].

There are six $\{10\bar{1}2\}$ planes and the commonly reported 38° $\langle 1\bar{2}10\rangle$ reorientation holds for secondary twinning on only one of these planes. The question thus arises as to why should this particular reorientation be so prevalent? It is not clear if it is physically favoured more than the other reorientations or if studies to date have simply overlooked the possibility of other reorientations. Indeed, Crocker's [13] analysis of double twinning on the $\{10\bar{1}1\}$ planes considered only the 38° $\langle 1\bar{2}10\rangle$ reorientation because of previous reports and the shared plane of shear. (That study was focused on rationalizing the final habit of the double twin, something that will not be considered in any detail here.)

A number of authors have found the Schmid factor to be useful in rationalizing observed twinning modes (e.g. [14,15]) and the present paper follows this line of investigation as a first attempt at examining the problem. To establish a statistically meaningful data set, the work draws on 30 EBSD maps of material tested in tension and compression and in both wrought and as-cast states. In what follows, the double twin variants are first identified, then the Schmid factors are calculated and summarized pictorially. This is followed by the presentation of our data and a comparison of the findings with predictions made using the Schmid analysis. Finally, some speculation is offered to explain why some of the results seem to be at odds with the Schmid predictions.

2. Background

2.1. Double twin variants

Here, we examine the reorientations that accompany primary $\{10\bar{1}1\}$ twinning followed by secondary $\{10\bar{1}2\}$ twinning. The objective is to identify the misorientation relations between the original matrix and the doubly twinned volume. The twinning reorientations were examined by manipulating matrix representation of the orientations according to standard procedures that can be found in the literature (e.g. [16]). The plane of shear of the twinning modes examined, $\{1\bar{2}10\}$, is a mirror plane and thus the twin reorientation can be performed by rotating 180° around the twinning plane normal [17].

The reorientations produced by the six secondary $\{10\bar{1}2\}$ twinning systems are illustrated in Fig. 2 on a pole figure (equal area projection), labelled A–F. The final orientations fall in three pairs. The members of each pair correspond to positive and negative rotations, in relation to the primary twin, of 86° around a single $\langle 1\bar{2}10\rangle$ axis. There are three of these axes, hence the three groups of final orientations. Furthermore, it turns out that the resulting misorientations between the initial matrix and the doubly twinned orientation are equivalent for twinning on planes C and E. The same is true for twin planes B and F. There are therefore four misorientation relations for us to consider and these are given in Table 1 in terms of angles and the nearest single-digit Miller indices. These relations are identified henceforth by the numbers **1**–**4** given in this table. The most commonly observed type discussed above corresponds to type **1**.

2.2. Schmid factor calculations

The Schmid factors for $\{10\bar{1}1\}$ twinning under uniaxial compression and uniaxial tension were calculated and the two most heavily stressed systems (in the sense that permits *c*-axis contraction) were subjected to further analysis. For

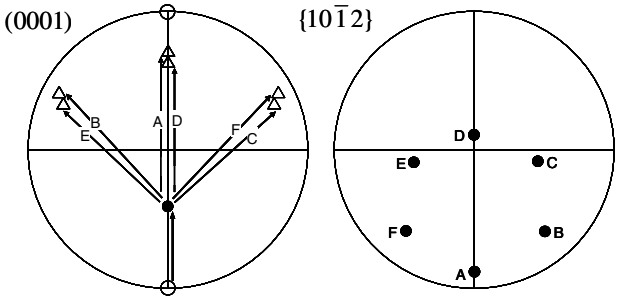

Fig. 2. (a) Reorientation of the basal poles during double twinning. The open circles refer to the original orientation, the closed circle refers to the reoriented basal pole produced after primary $\{10\bar{1}1\}$ twinning and the triangles reflect the final basal poles following secondary $\{10\bar{1}2\}$ twinning. (b) $\{10\bar{1}2\}$ twin planes after primary $\{10\bar{1}1\}$ twinning. The orientations produced by each twinning variant are tracked with the letters A–F.

Table 1
$\{10\bar{1}1\}$–$\{10\bar{1}2\}$ double twinning variants identified in the present study

Twinning variants	**1** (D)	**2** (A)	**3** (B and F)	**4** (C and E)
Misorientation relation	37.5° $\langle 1\bar{2}10\rangle$	30.1° $\langle 1\bar{2}10\rangle$	66.5° $\langle 5\bar{9}43\rangle$	69.9° $\langle 2\bar{4}21\rangle$
Colour on EBSD maps (on-line version)	Fuchsia or black	Green or white	Light blue	Dark blue

The capital letters refer to the secondary twinning planes identified in Fig. 2.

the orientations produced by these primary twin systems, the Schmid factors, m, for secondary $\{10\bar{1}2\}$ twinning were calculated. The secondary twin variants corresponding to the two systems with the highest Schmid factors were recorded. The favoured variants are identified in terms of the corresponding misorientation relation given in Table 1. The outcomes of these calculations are summarized in Figs. 3 and 4 for compression and tension, respectively. They are given in inverse pole figure space, which shows the orientation of the stress axis in the initial matrix (i.e. the parent orientation).

The occurrence of the different twinning variants clearly depends upon the whether the most heavily or second most heavily stressed twin system is considered. However, there are still some general comments that can be made. For compression along an axis close to the c-axis (i.e. for orientations that fall near the left-most corner of the inverse pole figures in Fig. 3), type **1** and **2** variants are expected. Conversely, for tension along an axis near to perpendicular to the c-axis, a deformation type encountered in tensile testing of rolled sheet and extruded bar, variants **3** and **4** are expected (Fig. 4).

The predictions in Figs. 3 and 4 are condensed further in Fig. 5 to give the broadest extent of the orientations where type **1** and **2** variants might be expected (non-shaded regions). The same is done for variant types **3** and **4**. It will be shown below that there is also some experimental benefit in these groupings.

3. Experiments

The material considered in the current study is commercial-grade magnesium alloy AZ31 (Mg–3%Al–1%Zn–0.2%Mn) obtained in three different forms: "as-cast", "extruded" and "rolled". The as-cast material, purchased in the form of a cast billet, possessed a random texture (as seen in Fig. 6a) and had an average linear intercept grain size of ~350 μm. The extruded material, purchased in the form of a 75 mm diameter bar, had an average linear intercept grain size of 8 μm and a strong axisymmetric texture, in which the majority of grains had their c direction normal to the extrusion axis (Fig. 6b). The rolled sheet was received with a thickness of 2.5 mm and had an average linear intercept grain size of 7 μm. The texture of the rolled sheet possessed a strong basal fibre component whereby a large volume fraction of grains were oriented with basal planes near to parallel to the rolling plane (Fig. 6c).

For both the as-cast and rolled material, machined samples were annealed for 2 h at 350 °C and air-cooled prior to deformation. Machined samples from the extruded material were tested in the "as-extruded" condition. Room-temperature tensile testing was conducted on all three materials to a range of strains up to failure. The as-cast material was also deformed in compression to a strain of 0.15 at room-temperature. EBSD was employed to examine the crystallographic reorientation caused by deformation

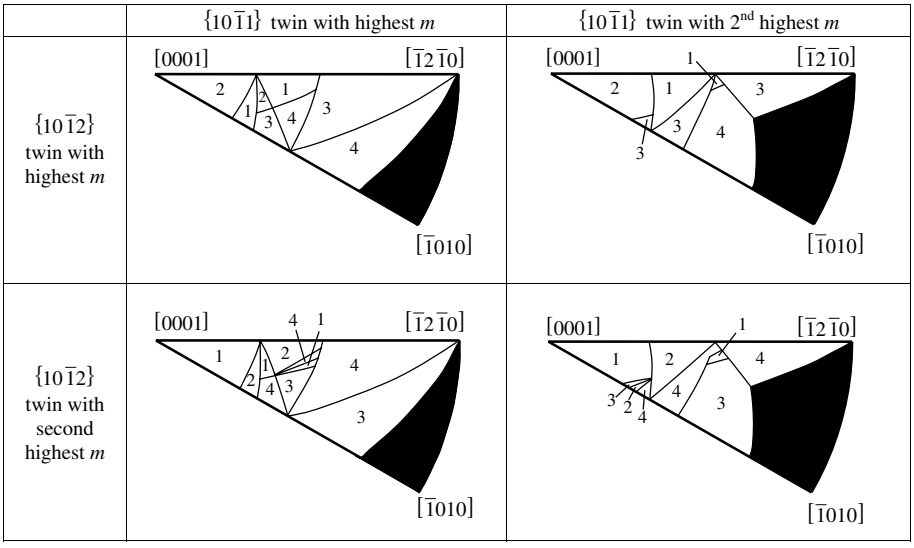

Fig. 3. Schmid factor (m) based predictions of secondary twin variants (**1–4**, see Table 1) in compression. The inverse pole figures reflect the orientation of the stress axis in the reference frame of the parent matrix. The dark regions are "forbidden" because of the polarity of twinning.

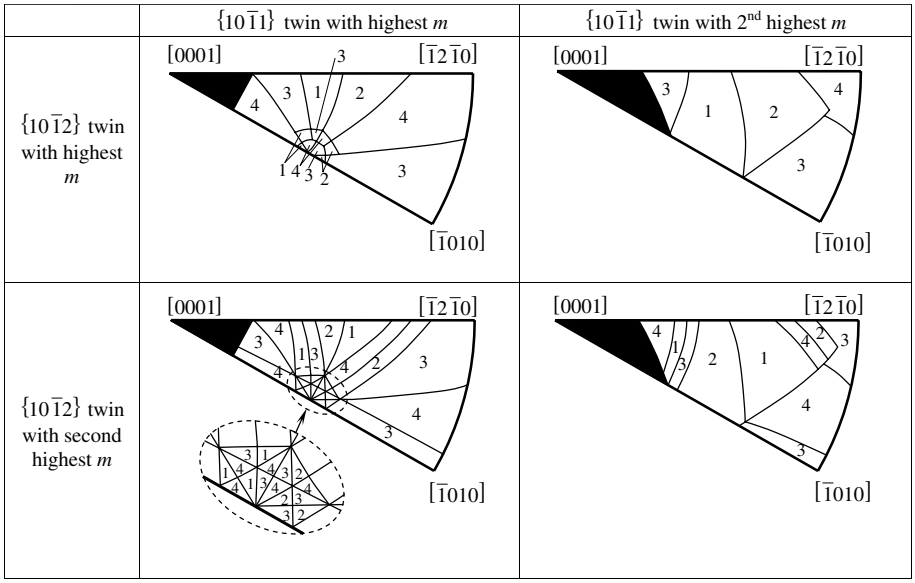

Fig. 4. Predictions of secondary twin variants in tension, plotted in the same manner as in Fig. 3.

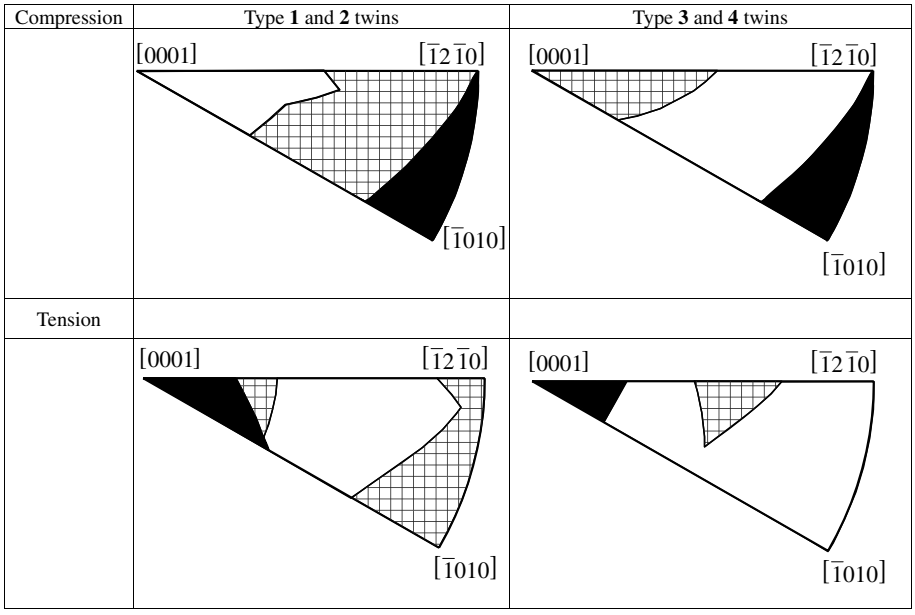

Fig. 5. Orientations of the stress axis where type **1** or **2** twins and type **3** or **4** twins are expected (unshaded areas). This is based on a consideration of the two most heavily stressed primary and secondary twin systems. The dark regions are "forbidden" and the hatched regions are "not predicted".

twinning. Samples were prepared for EBSD by grinding with 1200 grit SiC paper, diamond polishing through 6 and 3 μm, polishing with a colloidal silica suspension and then etching with a solution of 10 ml HNO_3, 30 ml acetic acid, 40 ml H_2O and 120 ml ethanol for 5 s.

4. Results

4.1. Observation of variants

EBSD maps produced from the experimental materials revealed examples of the four double twin variants identified above. Examples of each twin type are presented in Fig. 7. It is evident that the primary twin trace is near to that expected for the active $\{10\bar{1}1\}$ twin. The twin boundaries plotted were drawn by allowing an angular spread around the axis and angle of ±4°. The accompanying pole figures illustrate how the double twin variants **1** and **2** involve rotations around a common $\langle 1\bar{2}10\rangle$ pole. Types **3** and **4** involve rotations around different $\langle 1\bar{2}10\rangle$ poles for the primary and secondary twins.

The twinning can be complex, particularly in the coarser-grained cast samples. Overall, the number of primary $\{10\bar{1}1\}$ twins seen per grain varied between one and four. In two-thirds of the cases, one twin was seen per grain. Three or four twins were seen in 15% of the grains exam-

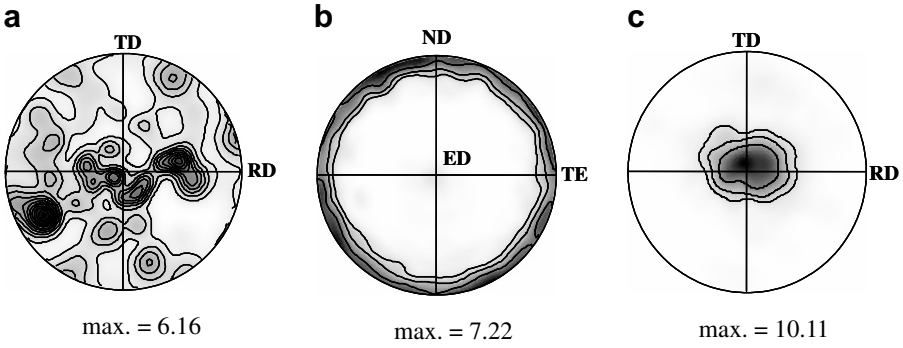

Fig. 6. Basal pole figures of (a) as-received as-cast billet (236 grains, intensity levels 0.5, 1, 2, . . .), (b) as-received extruded bar (intensity levels 1, 2, 4, 2768 grains) and (c) as-received rolled sheet (intensity levels 1, 2, 4, 178 grains).

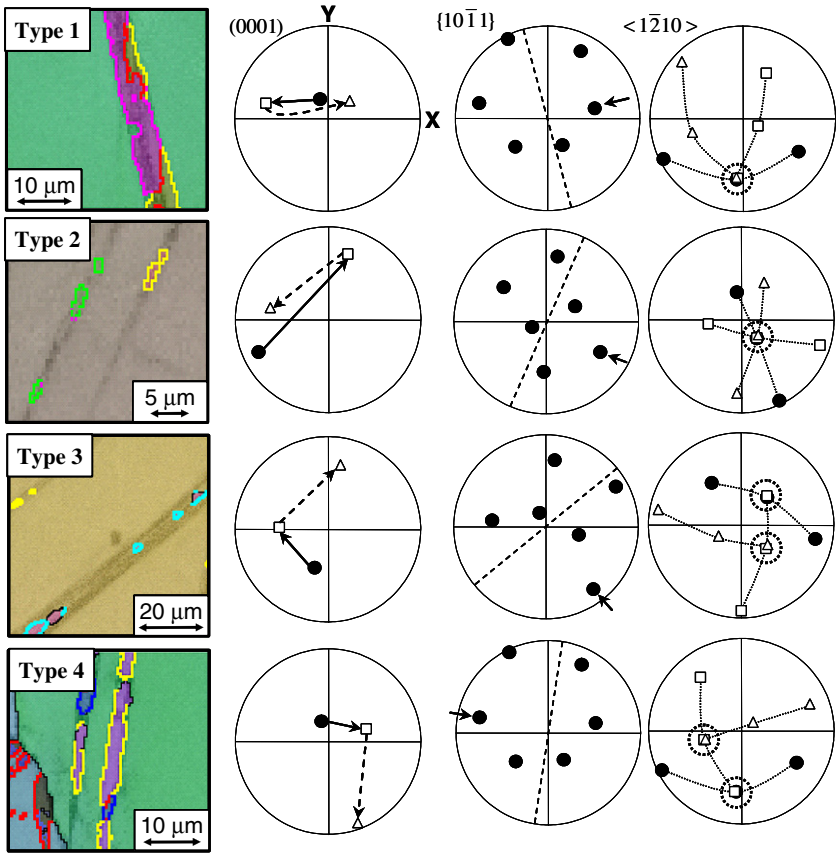

Fig. 7. EBSD measurements after tensile testing (in the horizontal direction) showing examples of the four double twin variants. Twin boundaries and twin types in EBSD maps identified as per Table 1 (Euler colouring – on-line version – and band contrast map components are included, with thin black lines representing random boundaries with misorientation >15°). In accompanying figures, dark circles represent the orientations of the parent grain, open squares represent the orientations of the primary twin and open triangles represent the orientations of the secondary twin. The active $\{10\bar{1}1\}$ twinning planes are also indicated by an arrow and their traces are dashed. The shared $\langle 11\bar{2}0\rangle$ axes are circled.

ined. No systematic increase in twin size was observed with the advent of secondary twinning and thus we saw no evidence for Crocker's suggestion [13] that the secondary twinning may aid twin growth.

Finally, in quite a number of cases, boundaries with a misorientation midway between twin variants **1** and **2** or **3** and **4** were observed. The most probable source of this discrepancy is the presence of additional deformation-induced lattice rotations. In some cases this is evident as an orientation gradient. An example of this is presented in Fig. 8. Shown are cumulative misorientations along parallel traces in and adjacent to a double twin. Uncorrelated misorientations of up to 3° are present. The corresponding boundary varies in misorientation between that assigned to the type **1** and that assigned to the type **2** misorientation variants (based on an allowance of ±4° about the angle

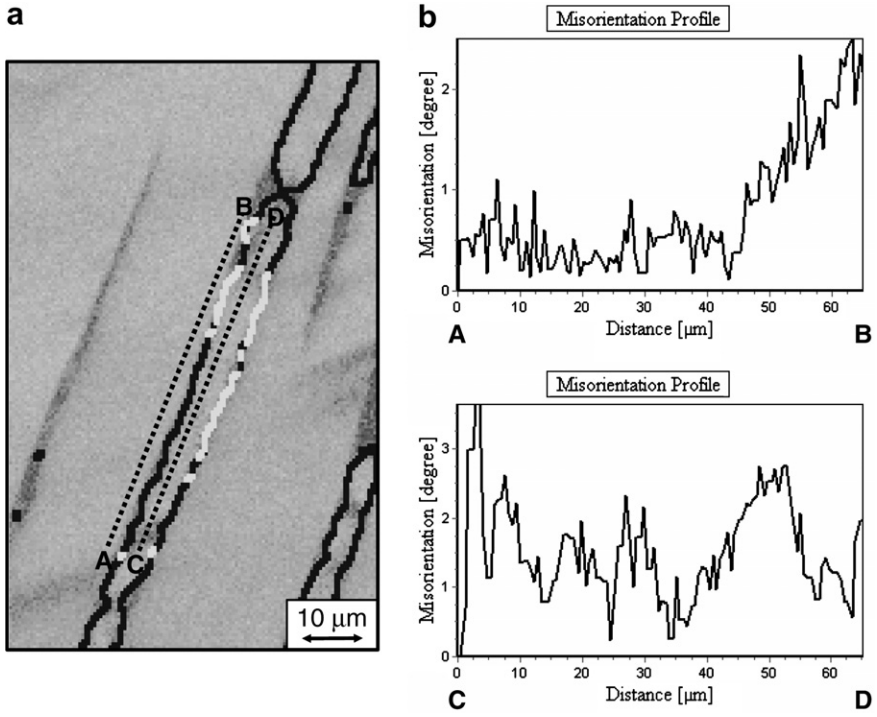

Fig. 8. An EBSD measurement revealing the spread in orientation along a $\{10\bar{1}1\}$–$\{10\bar{1}2\}$ double twin. (a) EBSD map, with twin boundaries identified as per Table 1 and (b) the cumulative misorientation along the dotted line from A to B (in the parent grain) and from C to D (in the doubly twinned region).

and axis). Such gradients introduce a degree of uncertainty into the present analysis. To acknowledge this uncertainty, the four secondary twin variants are grouped into two categories in much of the following analysis: type **1/2** and type **3/4**. Fortunately, this is quite consistent with the grouping of Schmid behaviours observed above. In general, the type **1/2** variant was found to be more common than type **3/4**. Also, cases of the type **1/2** variant consuming very high fractions of the primary twin volume were frequent.

4.2. Schmid factors for basal slip

The maximum Schmid factors (m) for basal slip within the doubly twinned volumes are compared with those of the corresponding matrix in Fig. 9 for all of the double twins examined in the present study. It is clear that this double twinning leads in a majority of cases to an increase in the Schmid factor for basal slip. The Schmid factor was raised by a factor >2 for just over a third of all cases. The mechanical consequences of this in single crystals were mentioned above and these have been examined in some detail for polycrystalline material by one of the present authors in Ref. [12].

4.3. Schmid factors and observed primary twin variants

The Schmid factors corresponding to the primary $\{10\bar{1}1\}$ twins were determined for all cases (130 of them) when the primary twinning system could be unambiguously identified. The distributions of Schmid factors according to value and rank are plotted in Fig. 10. The sign of the Schmid factors was assigned so that a negative value refers to the case where the sense of the resolved shear stress corresponds to that expected to cause contraction along the c-axis.

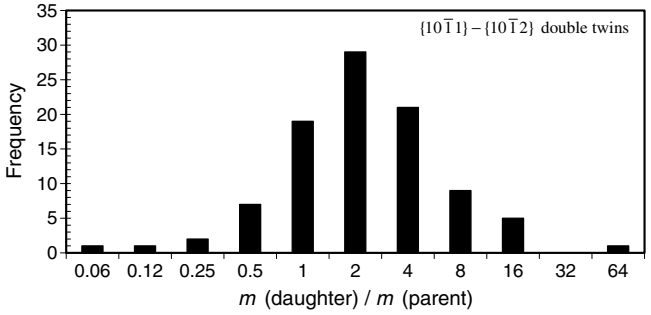

Fig. 9. Distribution of the ratios of Schmid factors (m) for basal slip before and after double twinning. In the majority of cases the Schmid factor increases significantly following twinning. (For the abscissa, the numbers given refer to the upper limits of the ranges used to establish the frequency.)

Approximately 60% of the primary $\{10\bar{1}1\}$ twins formed on systems with a negative Schmid factor >0.3. A small number of isolated instances were observed of twins forming on systems "forbidden" by the sense of the stress. In these cases, a nearby source of a departure from the imposed stress could be detected, such as an irregular grain boundary shape.

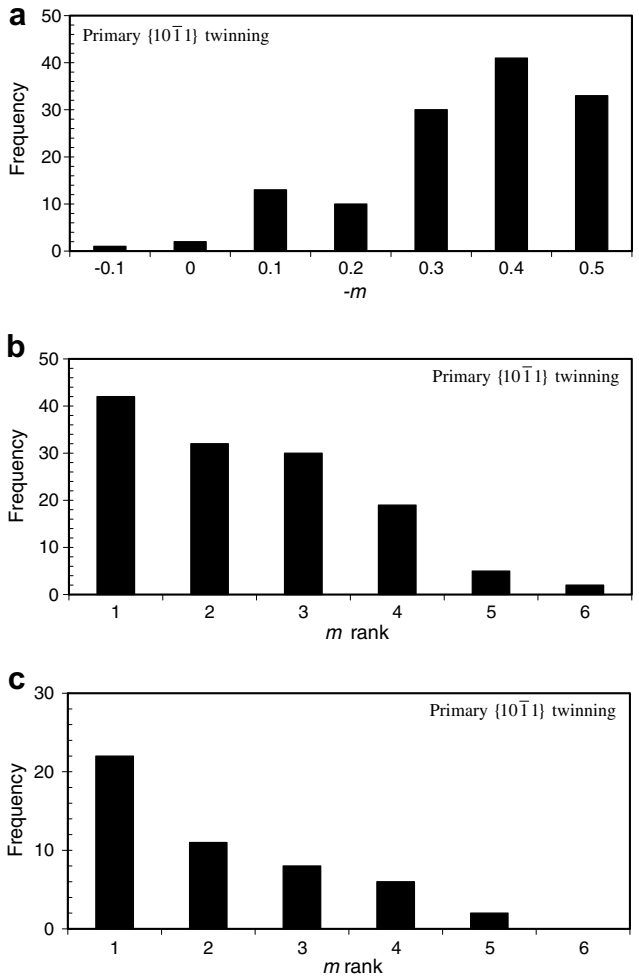

Fig. 10. (a) Schmid factor and (b) Schmid factor rank for all primary $\{10\bar{1}1\}$ twinning and (c) Schmid factor rank for $\{10\bar{1}1\}$ twinning for cases with one twin per grain.

In Fig. 10 it can be seen that ~55% of the primary $\{10\bar{1}1\}$ twins formed on either the most or the second most heavily stressed system. For cases where only one $\{10\bar{1}1\}$ twin was observed in the grain, this fraction increased to ~65%. It is clear that in these cases the Schmid factor is a reasonable predictor of the probability of primary twin formation. A fuller analysis employing crystal plasticity models is clearly desirable. For present purposes, we are interested in the behaviour of secondary twinning and this is examined below for a reduced data set of primary twins that formed on either the most or the second most heavily stressed primary twin system.

4.4. Schmid factors and observed secondary twin variants

The observed secondary twinning variants grouped into either the type **1/2** class or the type **3/4** class are plotted in Fig. 11 in the inverse pole figure space of the parent orientation. This manner of representation is chosen because it permits ready comparison with predictions (see Fig. 5). It is also avoids the need to determine the primary twinning reorientation, which in many cases is not available experimentally. It can be seen in Fig. 11 that there is reasonable agreement between experiment and the Schmid factor predictions in Fig. 5 for all conditions bar the occurrence of the type **1/2** variant in tension. The discrepancy for the type **1/2** variant is significant in that it accounts for the majority of the present cases.

For the type **1/2** variant in tension, >80% of the occurrences are on systems other than one of the two most heavily stressed systems (as determined by the Schmid factor). This is in contrast to the occurrence of the primary $\{10\bar{1}1\}$ twins considered above, where, for grains with one twin, ~35% of the time the twin formed on a system other than one of the two most heavily stressed systems. In other words, it appears that the type **1/2** secondary twin variant occurs more readily in tension than one would expect from a consideration of the Schmid factor.

To determine if there was a preference for the type **1** over the type **2** variant, the measured misorientation angles for twins in this category were examined. The histogram presented in Fig. 12 shows a clear skewing towards the type **1** variant. We can thus conclude that the emphasis on this variant in the literature is quite valid and that its occurrence appears to be anomalous in terms of a basic Schmid factor analysis.

5. Discussion

The over-representation of the type **1** secondary twin variant in the data obtained in tension is significant because it is the primary reason for the Schmid factor for basal slip to increase significantly following double twinning (see Fig. 9). The Schmid factors for basal slip in the doubly twinned regions were calculated for the ideal case where the most heavily stressed variants activated. In tension these were found to fall at values <0.2. In other words, if the type 1 variant was not favoured, one would not expect the Schmid factor to be increased so much by $\{10\bar{1}1\}$–$\{10\bar{1}2\}$ double twinning. Below, we explore some factors involved in the apparently non-Schmid dominance of the **1** variant by (i) considering the role of material condition, (ii) contrasting the phenomenon with the behaviour of primary $\{10\bar{1}2\}$ twinning and (iii) examining some mechanisms for enhanced growth of the type **1** twin.

5.1. Material condition

In the present work, data obtained using wrought and as-cast (and homogenized) material were combined. The main two differences between these categories of samples are: the grain size (coarser for as-cast material) and the texture (sharper for wrought material). To determine if this is important for the current observation, the data for the type **1/2** twin variants presented in Fig. 11 are replotted in Fig. 13 according to material type. It can be seen that there are high occurrences of the anomalous type **1/2** variant ("not predicted" in Fig. 5) present in both the extruded

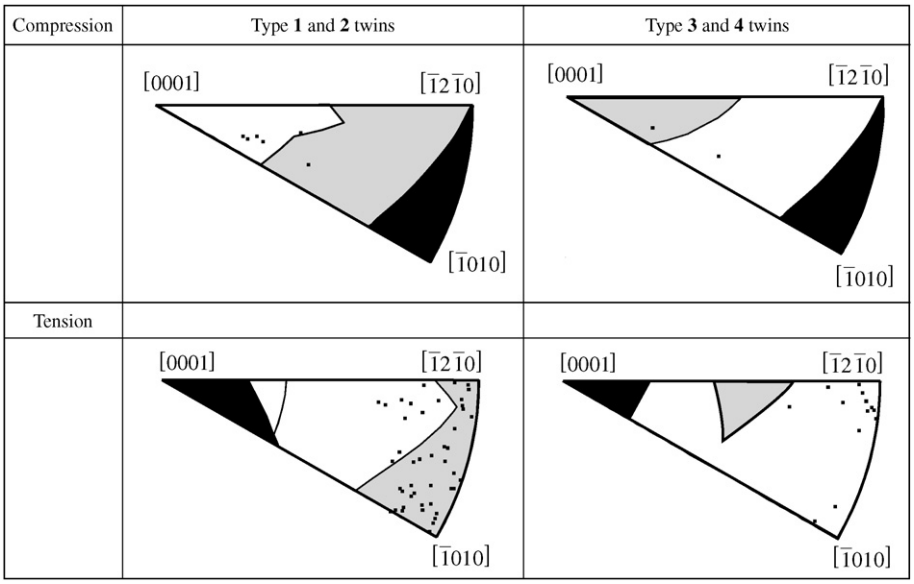

Fig. 11. Matrix orientations corresponding to the twin variants seen in the present study. The data shown are for secondary twinning occurring within primary twins that formed on the most or second most heavily stressed system. The shaded regions correspond to the "not predicted" regions in Fig. 5.

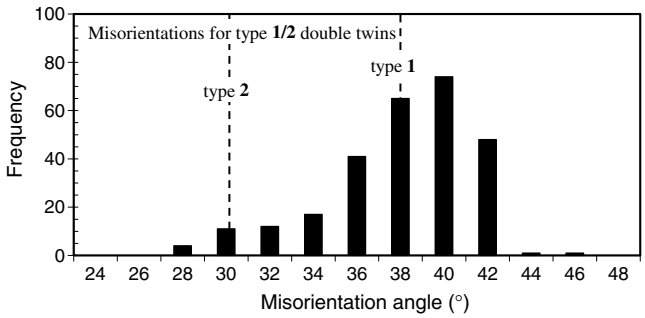

Fig. 12. Distribution of misorientation angles for double twins identified as being of the type **1** or type **2** class. There is a clear preference for type **1**. Two misorientation measurements per twin were employed to generate this plot.

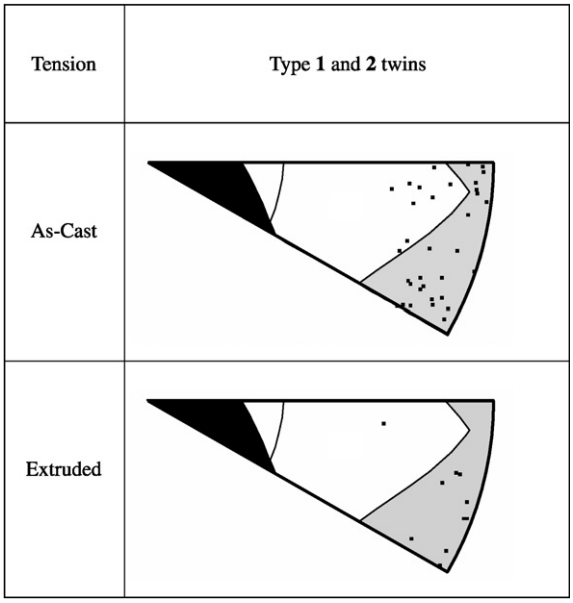

Fig. 13. Occurrences of the type **1/2** variant in tension separated according to the material condition. The regions shown correspond to those given in Fig. 5. Both conditions display non-Schmid behavior.

and the as-cast materials. We can therefore conclude that non-Schmid secondary twinning on the type **1** variant is probably not a phenomenon exclusive to coarse or fine grain sizes, or to sharp or weak textures.

5.2. Comparison with primary $\{10\bar{1}2\}$ twinning

The non-Schmid behaviour of secondary $\{10\bar{1}2\}$ twins contrasts with the formation of primary $\{10\bar{1}1\}$ twins, which agrees reasonably well with Schmid predictions. This may reflect a more general difference between the two twinning modes. To examine this possibility, the occurrence of primary $\{10\bar{1}2\}$ twinning in a sample of extruded AZ31 was inspected.

Extruded material was strained in tension perpendicular to the extrusion direction to a strain of ~0.04. The test direction was chosen to ensure a wide range of resolved shear stresses on the twinning planes. Extruded material was chosen because the fine grain size (~8 μm) provides more grains in the field of view during microscopy and a reduced contrast to the fine primary twinned regions that are the subject of the present paper. In all, 46 twins were examined and these were restricted to cases where one twin dominated the grain. The latter restriction was thought to more closely approximate the situation for secondary twinning, where one secondary twin is the norm.

The occurrence of $\{10\bar{1}2\}$ primary twins in extruded material can be seen (Fig. 14) to occur on planes with both a low Schmid factor magnitude and a low Schmid factor rank. In generating this plot, a judgement had to be made

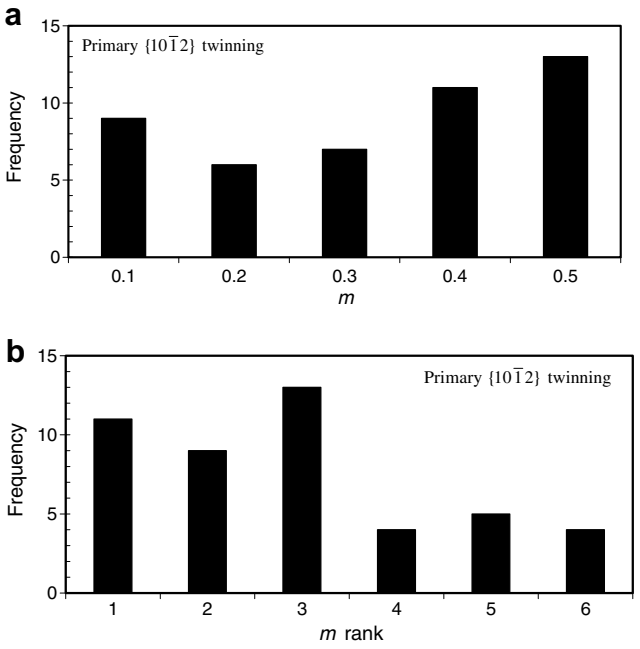

Fig. 14. (a) Schmid factor value and (b) Schmid factor rank for primary $\{10\bar{1}2\}$ twinning in extruded AZ31 bar strained in tension perpendicular to the extrusion direction for cases with one dominating twin per grain. (Rank 1 refers to twinning on the system with the most favourable Schmid factor and rank 6 to the least.)

for grains in which the parent orientation was not readily distinguished from the daughter orientation. For such cases, the orientation with the higher Schmid factor twinning was selected as the parent. This will tend to slightly overstate the adherence to the Schmid law.

One reason for the high frequency of $\{10\bar{1}2\}$ twinning on systems with low Schmid factors is that this mode is expected to have a lower critical resolved shear stress (CRSS) than for $\{10\bar{1}1\}$ twinning. For the present material, the CRSS for $\{10\bar{1}2\}$ twinning has been reported to fall in the range 30–50 MPa (e.g. [18,19]). An estimate for the value for $\{10\bar{1}1\}$ twinning can be made from the observation made by one of the present authors [12] that significant amounts of $\{10\bar{1}1\}$ twinning were seen to form in extruded material once the ultimate tensile stress of ~250 MPa was attained. The texture of extruded material is very sharp so an average Schmid factor of 0.4 is not an unreasonable estimate for $\{10\bar{1}1\}$ twinning. This gives a lower limit for the CRSS for $\{10\bar{1}1\}$ twinning of ~100 MPa, two to three times that seen for $\{10\bar{1}2\}$ twinning.

The key to understanding the significance of this observation is to recall that these twinning modes operate in competition with the basal and non-basal slip modes. The higher value of the CRSS for $\{10\bar{1}1\}$ twinning means that in grains where this mode finds itself poorly oriented there is a greater chance that one of the competing slip modes can activate instead. However, it is still not immediately obvious how one should understand the enhanced occurrence of $\{10\bar{1}2\}$ twinning on lowly ranked systems in place of a more highly ranked variant.

The lesser stressed (third or less most heavily stressed) primary $\{10\bar{1}2\}$ twinning systems account for ~55% of all the cases examined in Fig. 14. This is greater than the value obtained for the singly forming primary $\{10\bar{1}1\}$ twinning systems (35%), but still falls shy of the high (>80%) value obtained for the secondary **1/2** $\{10\bar{1}2\}$ systems. So, although it does appear that primary $\{10\bar{1}2\}$ twinning occurs more readily on the lesser stressed planes than for $\{10\bar{1}1\}$ twinning, the occurrence of the secondary $\{10\bar{1}2\}$ twinning on lowly stressed planes occurs even more frequently.

This difference is illustrated more vividly in Fig. 15. This figure presents the ratio between the Schmid factor of the observed and the Schmid factor of the most heavily stressed $\{10\bar{1}2\}$ twin variants. Normalizing in this manner gives an indication of the difference in stresses between the active and most heavily stressed variant. For primary $\{10\bar{1}2\}$ twinning (Fig. 15a), the active lowly ranked variants are not significantly less stressed than the most heavily stressed variant. This is consistent with the success of crystal plasticity modelling in capturing the key features of this twinning mode (e.g. [15,18]). For secondary $\{10\bar{1}2\}$ twinning, the situation is quite different (Fig. 15b). In the cases shown (which correspond to situations where the tensile stress is near to lying in the basal plane), the occurrence of the type **1** twinning involves activation of twin planes stressed considerably less than the most heavily stressed

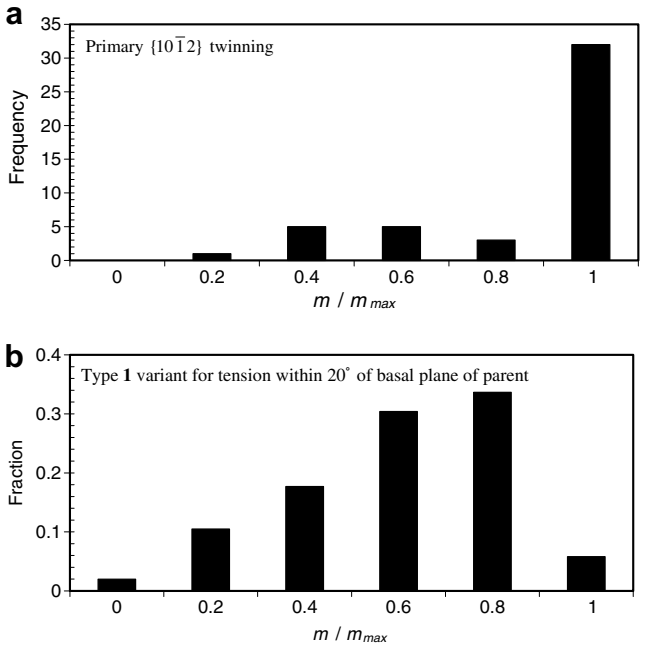

Fig. 15. Ratio between the Schmid factor of the active secondary twinning system and that of the most heavily stressed system for (a) the observed primary $\{10\bar{1}2\}$ twins and (b) for the type **1** variant for tension within 20° of the basal plane of the parent (i.e. the right-most region of the inverse pole figure). The formation of the type **1** variant for these orientations requires activation of twinning on planes that are significantly less stressed than the most heavily stressed system.

plane. It can thus be concluded that the predominance of the type **1** variant is a non-Schmid phenomenon that appears to be unique to secondary $\{10\bar{1}2\}$ twinning.

5.3. Possible variant selection mechanism

The calculation of the Schmid factor in the preceding analysis assumes that the local stress state is equivalent to the global stress state. This is not true in reality. Although it can provide a reasonable approximation in certain cases, it is less likely to be valid for the interior of thin lenticular primary $\{10\bar{1}1\}$ twins. However, it is not obvious *a priori* that this would favour any of the secondary $\{10\bar{1}2\}$ variants over any of the others.

Due to the inability of the EBSD technique to resolve fine newly formed secondary twins, it is not possible to say with any certainty that the present observation relates more to an enhancement of twin nucleation or to an enhancement of twin growth. However, irrespective of any particular preference for the nucleation of the type **1** variant, it is evident that once nucleated this variant displays a high rate of lateral growth. As mentioned above, many cases were seen where the type **1** variant consumed significant lengths of primary twin and no cases of obvious copious nucleation were seen at the present level of resolution.

One reason the type **1** variant might display an enhanced rate of growth has to do with the tendency of twins to minimize the compatibility strains. This principle explains the common lenticular shape of deformation twins with the short axis normal to the twinning plane and is described mathematically in the Eshelby inclusion problem [20]. In the case of lateral growth of secondary $\{10\bar{1}2\}$ twins, the final shape is enforced by the shape of the primary $\{10\bar{1}1\}$ twin. This leads to an increase in the compatibility strain. The greater the departure of the secondary twinning plane from the habit plane of the primary twin, the greater the additional compatibility strain. The higher the compatibility strain, the higher the expected impediment to secondary twin growth.

The angles between the primary and secondary twin planes for the four twinning variants are shown in Table 2. It can be seen that the two planes are significantly closer to coincidence for the type **1** variant than for any of the others. Thus one might expect that the stress for propagating the secondary twin throughout the primary twinned volume would be least for the type **1** variant. This may account for its over-representation seen in the present work.

Table 2
Angle between the primary $\{10\bar{1}1\}$ twin plane and the secondary $\{10\bar{1}2\}$ planes for each variant

Twinning type	1	2	3	4
Misorientation angle	18.8°	74.9°	87.6°	49.9°

Finally, it is also possible that the increased ease of basal slip in type **1** secondary twins serves to enhance their size and prevalence. This may occur through two ways. One is as a consequence of enhanced twin growth arising from the interaction of basal dislocations with the twin interface. This interaction can provide a ready source of mobile twinning dislocations [21]. Another is that the ease of basal slip in a newly formed doubly twinning volume may lead to local unloading, thus preventing the attainment of stresses required to form other secondary twin variants. To distinguish between these possibilities and identify others, more detailed characterization of these twins at higher resolutions is required.

6. Conclusions

(1) Inspection of the misorientations between the parent and $\{10\bar{1}1\}$–$\{10\bar{1}2\}$ doubly twinned volumes in magnesium reveals that there are four possible misorientation variants.
(2) Schmid analysis of $\{10\bar{1}1\}$–$\{10\bar{1}2\}$ double twinning in magnesium predicts that the variant formed should depend strongly on orientation and on whether tension or compression is employed.
(3) EBSD analysis of $\{10\bar{1}1\}$ primary twinning in Mg–3Al–1Zn magnesium alloy reveals good agreement with Schmid-type behaviour.
(4) EBSD analysis of $\{10\bar{1}2\}$ primary twinning in Mg–3Al–1Zn magnesium alloy reveals a behaviour that departs more from Schmid-type predictions than for $\{10\bar{1}1\}$ primary twinning. However, the occurrence of twinning on systems stressed considerably less than the most heavily stressed system is rare.
(5) The difference in behaviours between primary $\{10\bar{1}1\}$ and $\{10\bar{1}2\}$ twinning can be understood in part as a consequence of the differences in CRSS.
(6) The occurrence of secondary $\{10\bar{1}2\}$ twinning in primary $\{10\bar{1}1\}$ twins in tension favours the formation of misorientations characterized by 38° $\langle 1\bar{2}10\rangle$. For tension, this involves the activation of secondary twinning systems inconsistent with Schmid-type behaviour.
(7) One possible cause of the non-Schmid behavior of secondary twinning is that for the secondary twin to grow it must take on a shape enforced by the primary twin. This is non-optimal for strain compatibility. The 38° $\langle 1\bar{2}10\rangle$ variant provides the closest match between the primary and secondary twinning planes, thus minimizing the compatibility strain.

Acknowledgments

This work was funded by Deakin University, the ARC Centre of Excellence for Design in Light Metals and the ARC Discovery Grant scheme. Thanks to Andrew Sullivan, John Vella and Katrina Morgans for technical support. Helpful discussions with Sean Agnew (University of Virginia) are also gratefully acknowledged.

References

[1] Kelley EW, Hosford JWF. Trans Metall Soc AIME 1968;242:5.
[2] Wonsiewicz BC, Backofen WA. Trans Metall Soc AIME 1967;239:1422.
[3] Hartt WH, Reed-Hill RE. Trans Metall Soc AIME 1968;242:1127.
[4] Reed-Hill RE, Robertson WD. Int Metall Rev 1973;18:728.
[5] Roberts CS. Magnesium and its alloys. New York: John Wiley; 1960. p. 81.
[6] Yoshinaga H, Obara T, Morozumi S. Mater Sci Eng 1973;12:255.
[7] Barnett MR, Nave MD, Bettles CJ. Mater Sci Eng A 2004;386:205.
[8] Nave MD, Barnett MR. Scripta Mater 2004;51:881.
[9] Couling SL, Pashak JF, Sturkey L. Trans ASM 1959;51:94.
[10] Hartt WH, Reed-Hill RE. Trans Metall Soc AIME 1967;239:1511.
[11] Jiang L, Jonas J, Luo A, Sachdev A, Godet S. Scripta Mater 2006;54:771.
[12] Barnett MR. Mater Sci Eng 2007;464:8.
[13] Crocker AG. Philos Mag 1962;7:1901.
[14] Reed-Hill RE. In: Reed-Hill RE, Hirth KP, Rogers HC, editors. TMS-AIME conference, deformation twinning, vol. 25. Gainesville, FL: American Institute of Mining, Metallurgical and Petroleum Engineers; 1964. p. 295.
[15] Godet S, Jiang L, Luo AA, Jonas JJ. Scripta Mater 2006;55:1055.
[16] Bunge HJ. Texture analysis in materials science. London: Butterworth; 1982. p. 1.
[17] Christian JW, Mahajan S. Prog Mater Sci 1995;39:1.
[18] Jain A, Agnew SR. Mater Sci Eng 2007;462:29.
[19] Barnett MR. Metall Mater Trans A 2003;34A:1799.
[20] Lebensohn RA, Tome CN. Philos Mag A 1993;67:187.
[21] Serra A, Bacon DJ. Philos Mag A 1996;73:333.